12th International Conference on Fracture Mechanics of Concrete and Concrete Structures
FraMCoS-12
B.L.A. Pichler, Ch. Hellmich, P. Preinstorfer (Eds)

https://doi.org/10.21012/FC12.1166
TT-C1:4

FRACTURE MECHANISM AND INTERFACE BEHAVIOR OF PRESTRESSED SEGMENTAL UFC BEAMS WITH A CIRCULAR CROSS SECTION UNDER BENDING

MAMY A. RABOTOVAO[*], TOMOHIRO MIKI[†]

[*] Kobe University, Department of Civil Engineering
1-1 Rokkodai, Nada, Kobe 657-8501, Japan
e-mail: 207t137t@stu.kobe-u.ac.jp

[†] Kobe University, Department of Civil Engineering
1-1 Rokkodai, Nada, Kobe 657-8501, Japan
e-mail: mikitomo@port.kobe-u.ac.jp

Key words: Fiber Reinforced Concrete, Normal Concrete, Fiber content, Prestressed Hollow Tubular Beams

Abstract: This research investigates the behavior of concrete tubular segmental beams prestressed with PC bars, focusing on the load-deflection characteristics and failure mechanisms. The interface parameter obtained from experimental results provides insight into modeling the epoxy joints used in large wind turbine towers. Specimen S8-JI2 exhibited failure patterns, load-deflection behavior, and tensile stress comparable to those observed in the experimental specimen. A unique failure mode dominated by longitudinal cracks was observed, explained by the arch mechanism activated when the interface joint opened. This led to a shift in the neutral axis, resulting in compressive stress transfer within the UFC and generating lateral stresses, which caused horizontal cracks. The study also found that reducing steel fiber content from 2% to 1.2% resulted in reduced load-carrying capacity and altered failure patterns, with the arch mechanism becoming more prominent in the lower fiber content specimen. Additionally, normal concrete specimens exhibited pronounced diagonal cracking due to interface opening, particularly in the central segment of the beam.

1 INTRODUCTION

UHPC exhibits good mechanical properties, strain-hardening behavior after cracking, and excellent durability [1-3]. Hence, UHPC is considered one of the most promising construction materials for future sustainable and resilient infrastructure [4]. However, owing to its low water-to-binder ratio (W/B, 0.15 to 0.25), UHPC exhibits high autogenous shrinkage at early ages, accompanied by strong hydration. The shrinkage and creep of UHPC, which are harmful to structures, can be significantly reduced through prior heat treatment [5]. Therefore, UHPC is expected to be applicable for structural components produced in industrial precast factories to achieve high strength, good durability, and low shrinkage and creep.

Recently, precast concrete (PCa) segmental bridges with hybrid tendons and epoxy joints have become increasingly popular. PCa segmental bridges with hybrid tendons and dry joints are considered a competitive alternative for rapid construction. However, due to the stress concentration at the dry joints, the ultimate strength of segments with dry joints could be less than that with epoxy joints [6]. The epoxy joints possess a higher shear-resistance capacity and better durability than dry joints. In addition, epoxy resin as a lubricant can mitigate the fixing of imperfections

between the segmented surfaces [7]. Epoxy joints should be designed to have sufficient capacity to transfer shear force, axial force, and bending moments under static and dynamic loading [8].

The epoxy joint between the modeled PCa UHPC segments has a surface-to-surface interaction with two contact properties, including two types: normal behavior and shear behavior. A hard contact type was adopted as the normal behavior; in other words, the amount of stress transfer in the interface was not limited. A Coulomb friction model with a friction coefficient of 0.7 was adopted for shear behavior. In both normal behavior and shear behavior models, when the pressure in the interface was zero or negative, the two contact surfaces split. The author concluded that numerical simulation analysis of large-sized PCa UHPC segmental beams requires the investigation of more interface parameters to understand the flexural load-bearing capacity of those members [9].

It investigated the effect of different normal and shear stiffness moduli of the interface, on the behavior of UFC beams. The shear stiffness modulus did not affect much of the behavior of the tubular segmental beams. The one that was predominant was the normal stiffness modulus [10].

2 ANALYTICAL PROGRAMS

2.1 Analytical specimens

The analytical program compares the experimental specimen to different specimens. The geometry of those specimens is shown in **Figure 1** and **Figure 2**. The details of the analytical specimens are summarized in **Table 1**. Each specimen is 10 meters long, with an external diameter of 1000 mm and a thickness of 70 mm. The specimens were modeled in 3D with DIANA ver.10.7. The analytical program combined monolithic and segmental specimens to understand the effect of those joints on the bending behavior of Segmental UFC hollow circular beams. Different prestress levels 4 N/mm^2, 8.54 N/mm^2, and 12 N/mm^2 are also investigated.

Regarding the boundary conditions, two lines were drawn at the bottom faces of both supports (support left and right). The left support of the beam was fixed in all directions, X, Y, and Z on that line. The right support was only fixed in two directions, Y and Z. Moreover, it is suggested that the displacement along the Y axis of the bottom faces of both supports is fixed, as well as the rotation of those faces around X and Z directions (this is done so that the support plates marry the movement of the beam during the loading).

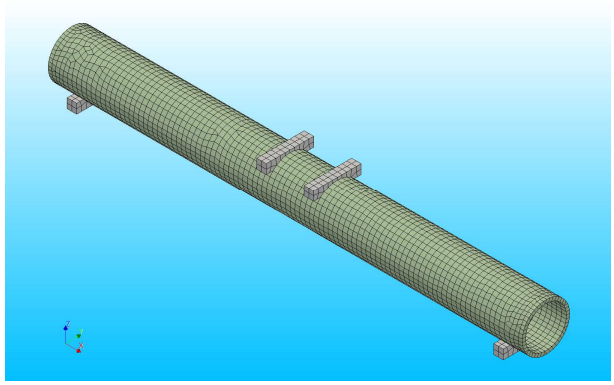

Figure 1: Monolithic specimen

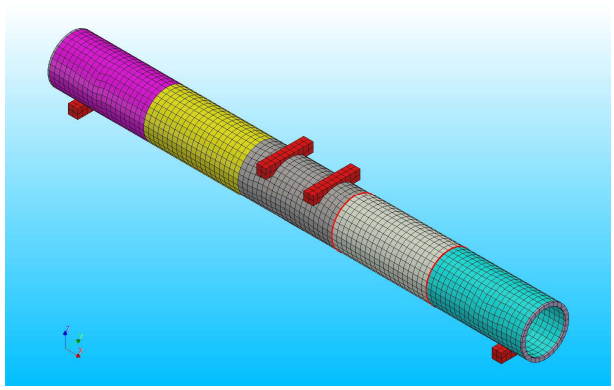

Figure 2: Segmental specimen

2.2 UFC models

Regarding the material properties, the UFC formulation incorporated steel fibers to enhance the structural integrity of the beam. These fibers, which had a diameter of 0.2 mm and a length of 15 mm, were used at a composition rate of 2.0% by volume.

The constitutive models of UFC are shown in **Figure 3** and **Figure 4**, respectively, for the

Table 1: Specimens

Type of specimen	Designation	Length (m)	Thickness (mm)	Prestress (N/mm^2)
Segmental	Exp	10	70	8.54
Monolithic	M-8	10	70	8.54
Segmental	S8-JI1	10	70	8.54
	S8-JI2	10	70	8.54
	S8-JI3	10	70	8.54

compressive and tensile behavior. The compressive and tensile behaviors of UFC were based on the specification of JSCE. The measured compressive strength is 180 N/mm^2. The measured modulus of elasticity of UHPC during the experiment is 46 000 N/mm^2. The tensile strength of concrete was 8.8 N/mm^2. Moreover, for the tensile behavior of UFC, $,\varepsilon_{cr}, \varepsilon_1$ and ε_2 are 0.0001913, 0.013 and 0.109 respectively. A total-based cracked model is associated with the UFC concrete. Based on JSCE specification, the compressive strength and tensile strength of UFC used in the analysis are:

$$f_c = 0.85 f'_{ck}/\gamma_c \quad (1)$$

$$f_t = f_{tk}/\gamma_c \quad (2)$$

where $f'_{ck}$is the measured compressive strength of concrete, f_{tk} is the measured tensile strength of concrete, and γ_c is a safety factor equal set as 1.0 in this study.

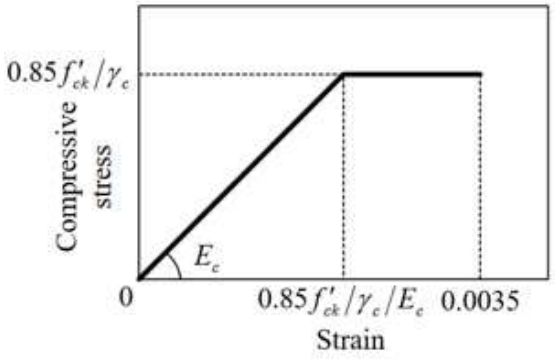

Figure 3: Compressive behavior of UFC

Regarding the tensile behavior of the UFC, the tension softening diagram (TSD) indicates this relationship between stress transfer and the crack width. The tension softening diagram is an important property to verify the structural safety of UFC members for ULS. For the design purpose of the ULS, the TSD, which includes the tensile strength and crack mouth opening displacement (hereafter referred to as CMOD) is given. The characteristic tensile strength f_{tk} becomes 8.8 N/mm^2, CMOD for which a certain stress level is retained after the first crack w_{1k}= 0.5 mm, and CMOD for which the stress comes to zero w_{2k} = 4.3 mm.

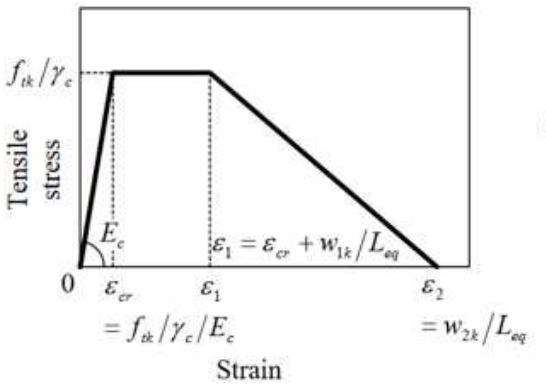

Figure 4: Tensile behavior of UFC

2.3 Normal concrete model

The behavior of concrete in compression was modeled using the stress-strain of the parabolic model as shown in **Figure 5**. The area below the softening part of the compressive stress-strain curve equals to G_c/h . The compressive strength of concrete was set as 36 N/mm^2. The characteristic length h was taken as 50 mm. The compressive fracture energy G_c of 53 N/mm was calculated as follows:

$$G_c = 8.77\sqrt{f'_c} \quad (3)$$

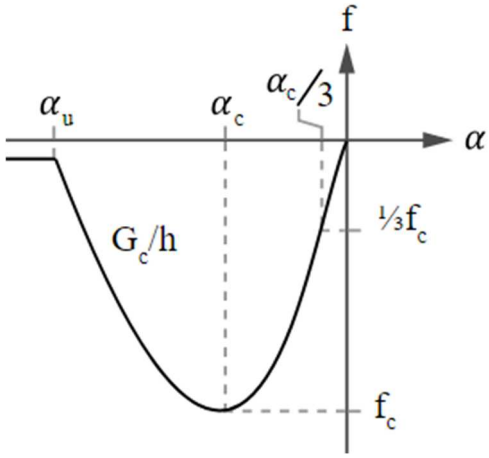

Figure 5: Compressive behavior of normal concrete

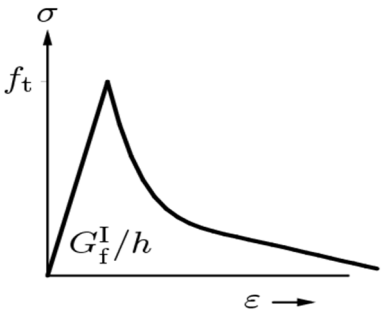

Figure 6: Tensile behavior of normal concrete

For the stress-strain relationship of concrete subjected to tensile stress shown in **Figure 6**, the Hordjik model was adopted. The tensile strength of concrete was set as 2.5 N/mm^2. The Hordjik model was adopted.

2.4 PC bar model

The PC bars used during the experiment had a yielding strength of 1175 N/mm^2 and a tensile strength of 1785 N/mm^2, corresponding to an ultimate strain of 0.03. Each PC bar had a diameter of 13 mm, and each specimen was reinforced with 18 PC bars.

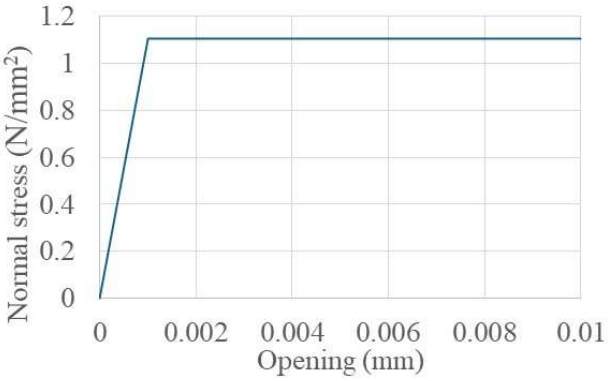

Figure 7: Normal stiffness modulus for interface

2.5 Interface models

A surface-to-surface connected interface elements were considered to reproduce the joint between two segments. This surface-to-surface interface element was defined between two solids' touched surfaces. Normal and shear stiffnesses are assigned to these surfaces.

The normal and shear stiffness moduli of the interfaces define the opening and sliding of the joint during the loading. Those parameters were calculated based on the bending theory with the assumption that during the elastic phase of the loading, the opening of the interface is small enough to allow the stress transfer among the UFC segments. Therefore, the normal stiffness moduli and shear stiffness moduli of the interface can be considered as the increment in stress (shear and normal stresses) in the monolithic specimen divided by the opening and sliding observed during the experiment.

The calculated normal stiffness modulus is 1105 N/mm^2 for an opening of 0.0008 mm, as shown in **Figure 7**. A normal stiffness reduction close to 0 must be considered to model the plateau. In this paper, values of 0.0005, 0.001, and 0.01 are considered.

Table 2: Interfaces parameters

Designation	Interface type	Normal stiffness modulus (N/mm^3)	Shear stiffness modulus (N/mm^3)	Normal stiffness reduction factor
JI1	NE	1105	25	0.0005
JI2	NE	1105	25	0.001
JI3	NE	1105	25	0.01

*NE: Non elastic interface

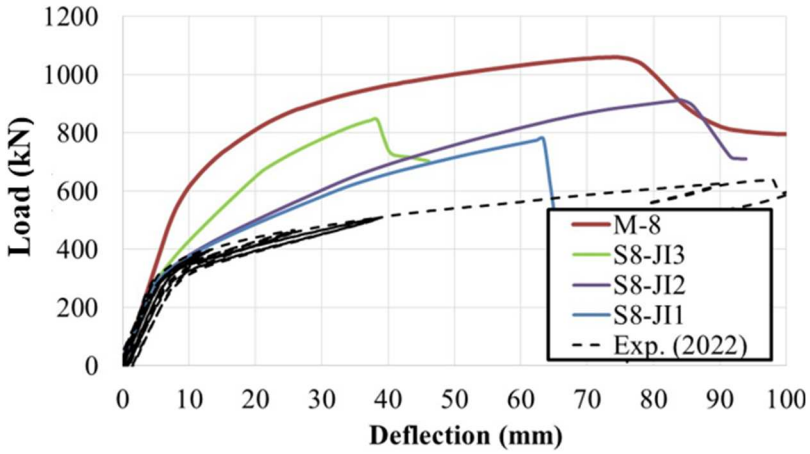

Figure 8: Effect of the interface parameters on the load deflection

3 VALIDATIONS OF THE INTERFACE PARAMETERS

3.1 Load deflection curves

Figure 8 shows the effect of the stiffness reduction factors on the load-deflection curves of hollow segmental circular UFC beams. In this analytical program, the reduction factors of 0.01, 0.001, and 0.0005 all represent a plateau after the critical opening of the interface. However, it is important to understand which parameter is more suitable for the ongoing investigation of the bending behavior of UFC hollow segmental beams. Segmental specimens are considered to observe the effect of those reduction factors.

For the experiment, the displacement was measured at the center point of the load and at the joint (between No. 2 and 3, No.3 and 4). In the loading test, the epoxy resin applied to the axial joint peeled off at the stage when the introduction prestress was exceeded, and the joint was opened.

The load deflection curves above show that the bilinear behavior with a second flexural stiffness is observed in specimens with a reduction factor. Based on the figure above, as the reduction factor decreases, the second flexural stiffness of the specimens is reduced.

However, the reduction factor 0.01 with specimen S8-JI3 presents a better flexural stiffness than the two cases, whereas the drop of load carrying capacity occurs faster. The peak load was 846 kN.

The reduction factor of 0.0005 leads to a low load carrying capacity and a failure at 65 mm with a load of 779 kN for the specimen S8-JI1. Among the three cases, the reduction factor of 0.001 presents a deflection close to the experimental specimen. The specimen S8-JI2 reaches a more significant deflection than the other two.

All the analytical results present a higher second flexural stiffness than the experimental result due to the contribution of the PC bars. Reproducing the ungrouted situation in the experiment.

Regarding strength, the higher the reduction factor, the stronger the interface joint. Based on these load-deflection curves, the reduction factor of 0.001 is more suitable to represent the epoxy joint used during the experiment.

3.2 Cracking pattern at P 345 kN

Two different loading stages, 345 kN and 700 kN, are considered to understand the effect of the stiffness reduction factor on the interface. **Figure 9** shows the cracking patterns of different specimens at a loading of 345 kN. The cracking patterns of specimens at a loading of 345 kN show that the monolithic specimen presents several flexural cracks at this stage; in the other hand, all segmental specimens' flexural cracks are absorbed by the opening of

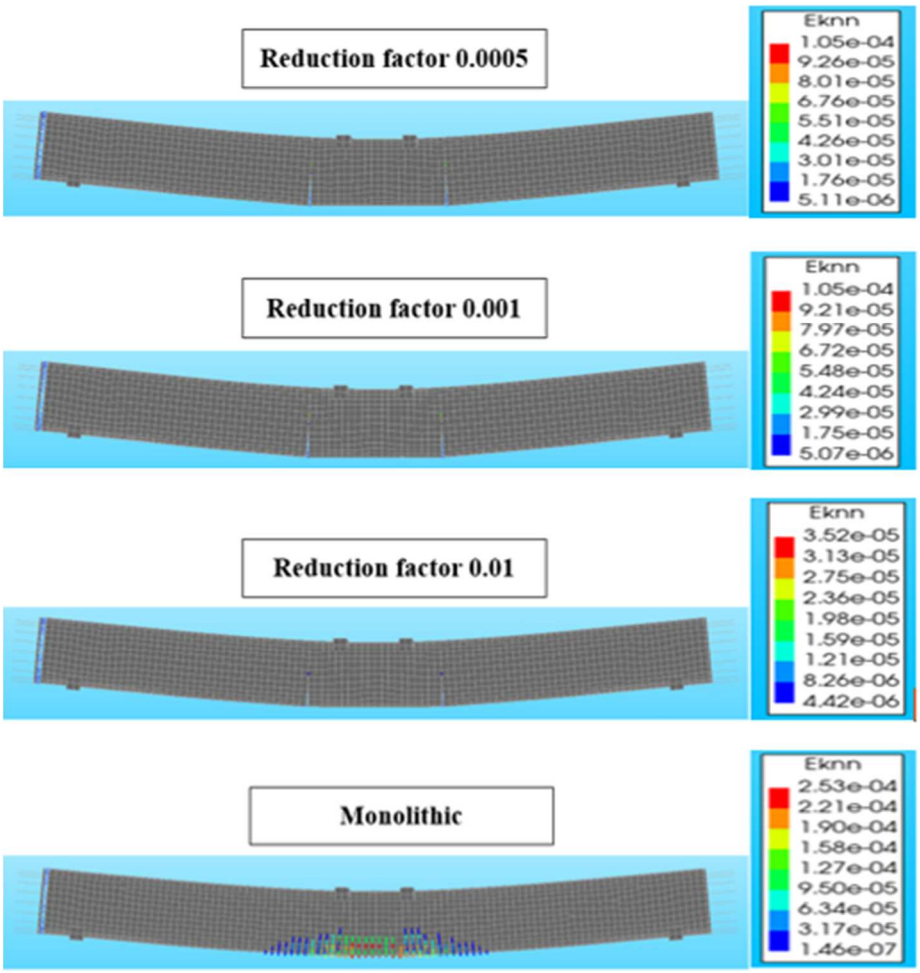

Figure 9: Cracking pattern at P - 345 kN

the joint interface, regardless of the value of stiffness reduction factor.

3.3 Cracking patterns P 750 kN

Figure 10 shows the cracking propagation of all the specimens for a loading of 750 kN. The monolithic specimen shows a bending behavior since the apparition of more flexural cracks in the body of concrete. The segmental specimens present almost the same cracking patterns. As the joint interface keeps opening, the middle segment of the beam presents several flexural cracks. Some differences were observed as the stiffness reduction factor increased. The stiffness reduction factors of 0.0005 and 0.001 lead to some flexural cracks in the middle segment of the beam, but the horizontal cracks in the compressive side of the cross-section of the beam, are more dominant with Eknn of 0.00291 and 0.00281; such are the cases for S8-JI1 and S8-JI2 respectively. The same situation was observed during the experiment. Horizontal cracks appear first due to the joint interface opening, resulting in large stresses at the location where the joint interfaces are not open yet, resulting in horizontal cracks. After the appearance of those horizontal cracks, flexural cracks occur as the middle segment of those specimens behaves as an independent beam.

On the other hand, a specimen with a stiffness reduction factor of 0.01 presents some horizontal cracks, but flexural cracks are the dominant one since the Eknn of flexural cracks is the highest for this case. The specimen S8-JI3, with a reduction factor of 0.01, shows that as the opening of the joint interface occurs, flexural cracks are observed in the middle segment of the specimen. The intensity of those flexural cracks increases as it goes to the middle of the segment with an Eknn of 0.00187.

The monolithic specimen tends to show

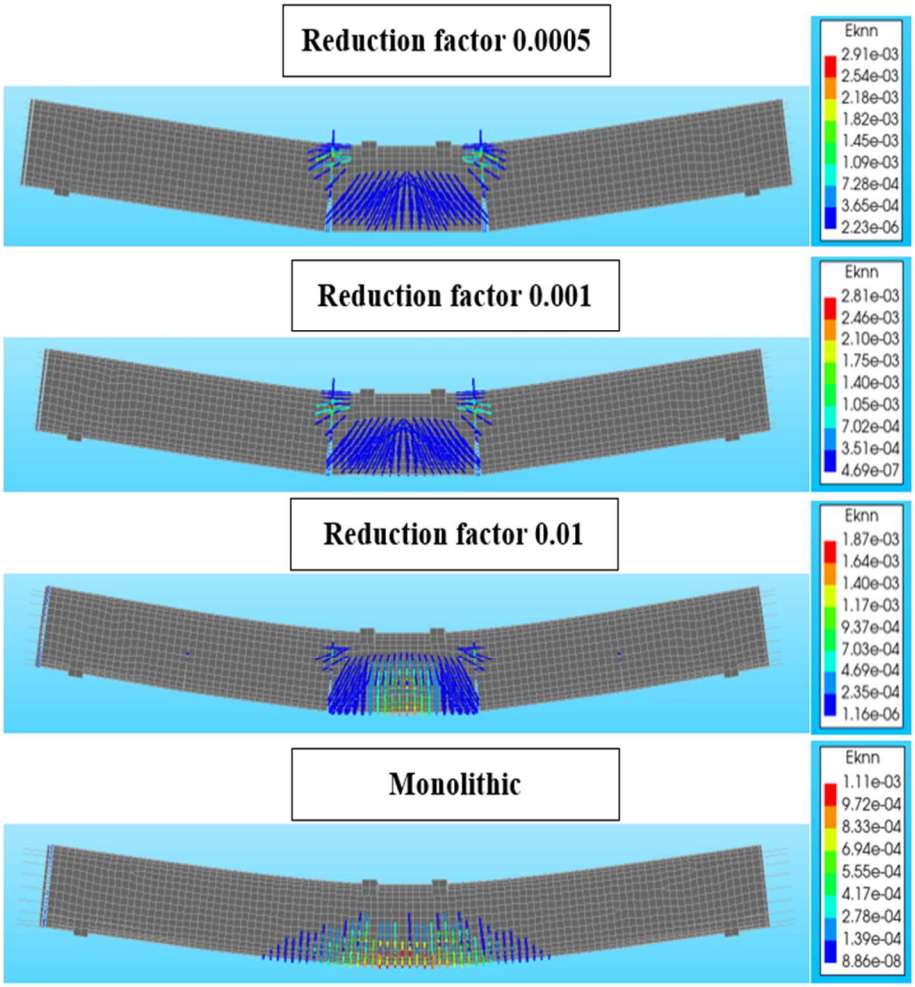

Figure 10: Cracking patterns at P – 750 kN

several flexural cracks at a low intensity with an Eknn of 0.0011. The lowest Eknn among all the specimens, it shows a better cracking strain distribution in the body of concrete.

3.4 Failure pattern

Analytical results show different cracking patterns as the stiffness reduction factor varies from one specimen to another, as shown by **Figure 11**. Starting with the stiffness reduction factor of 0.0005, specimen S8-JI1 shows flexural cracks with a specific angle that are more concentrated on the middle segment of the specimen. Moreover, large horizontal cracks with an Eknn of 0.00343 are observed in the compressive side of the specimen.

For the stiffness reduction factor of 0.001, the flexural cracks of the specimen S8-JI2 are also concentrated in the middle segment of the specimen. This time, those flexural cracks present a higher intensity in the middle of the beam with an Eknn of 0.0103. Some horizontal cracks are also observed in the compressive side of the beam.

With a reduction factor of 0.01, specimen S8-JI3 presents several flexural cracks in the middle segment of the beam, with a difference of predominant bending cracks leading to the drop of load carrying capacity of the specimen. Moreover, some flexural cracks start to propagate in the segments N02 and N04 of the specimen.

The monolithic specimen presents a bending failure.

3.5 Tensile strain in the PC bars

This section presents the tensile strain in the PC bars. These tensile strains in the PC bar were measured directly under the loading location. During the experiment, the initial measurement

Table 3: Tensile strain in the PC bars

ID	Strain (μ)
Exp	6200
S8-JI1	11500
S8-JI2	9300
S8-JI3	6700

of PC strain was carried out after completion of the post-tensioning. A tensile strain of 3770 microstrains (tensile strain generated by the jacking process of the PC bars) is added to the tensile strain of the PC bar at the peak load (for the experimental result only).

The result shown in **Table 3** is that for all the specimens, experimental or analytical, the tensile strains in the PC bars do not reach the ultimate tensile strain of 30000 microstrains; therefore, the failure of these specimens is related to the PC bars.

By comparing the tensile strain of these two specimens (Exp. (2022) and S8-JI2), S8-JI2 shows more contribution from the PC bars than the experimental specimen, allowing it to reach a higher load-carrying capacity, respectively 912 kN and 637.2 kN for S8-JI2 and the experiment.

Regarding the specimens S8-JI1, the PC bars contributed largely to the resistance of the specimen during the bending. This is due to the fact that S8-JI1 presents a stronger interface and, therefore, a smaller opening of the interface during the loading, leading to a better stress transfer. However, this led to an early failure at a deflection of 45 mm.

For S8-JI3, the PC bars presented a tensile strain of 6700 microstrains, almost like that of the experimental specimen.

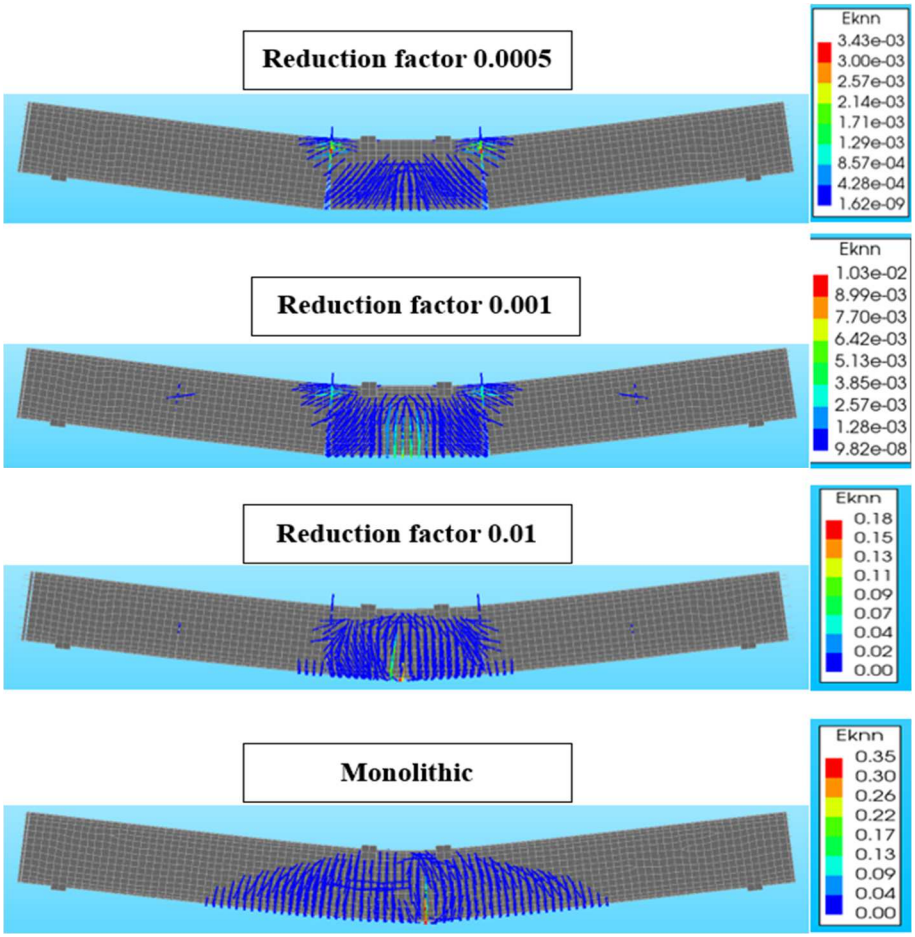

Figure 11: Failure patterns

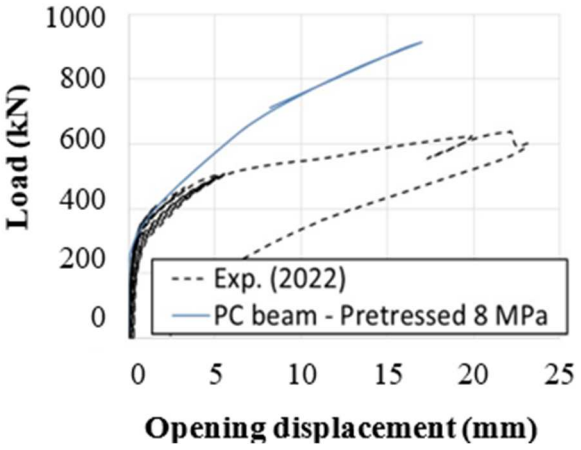

Figure 12: Interface opening

3.6 Validation and choice of interface parameters

The analytical results show that the joint interface model JI2 provides closer results to the experimental one. Therefore, it will be considered the main parameter for the joint interfaces in the following.

3.7 Interface openings

Figure 12 presents the opening of the joint in the middle of the beam in the bottom part for the experiment and the analytical case. Analytical specimens present a larger flexural stiffness compared to the experiments and both cases almost present the same pattern regarding the opening of the interface. The behavior of the opening of the interface could be decomposed into three phases. The elastic phase, all specimens present similar behavior in that phase. Then the second phase, which both cases present the same behavior too. However, in the third phase, a

4 EFFECTS OF THE TENSILE FRACTURE ENERGY G_F ON THE BEHAVIOR OF THE SPECIMENS

In this section, three different concrete materials are considered: normal concrete, UHPC with a fiber content of 1.2%, and UFC with a fiber content of 2%.

4.1 Load carrying capacity

The load carrying capacity of the three different specimens shows a totally different trend. As can be seen in Figure 13, the specimen with a fiber content of 2% presents the best load carrying capacity.

Specimen with a fiber content of 1.2% presents the same flexural stiffness as the specimen with 2% fiber content up to 45 mm deflection, at this stage, a drop of load carrying capacity is observed. After the drop, the structure reaches a very large deflection.

For the normal concrete specimen, the structure reaches a maximum deflection of 28 mm. The flexural stiffness of the specimen

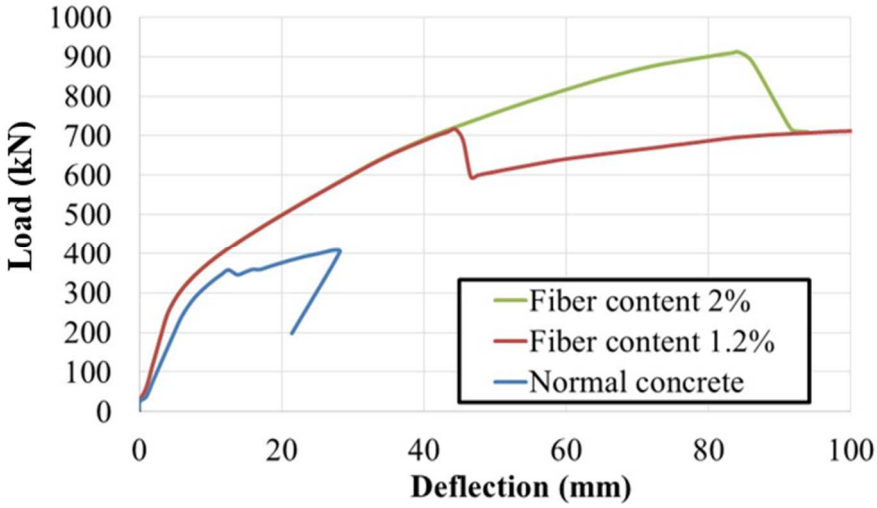

Figure 13: Effect of fiber contents on the load-deflection curves

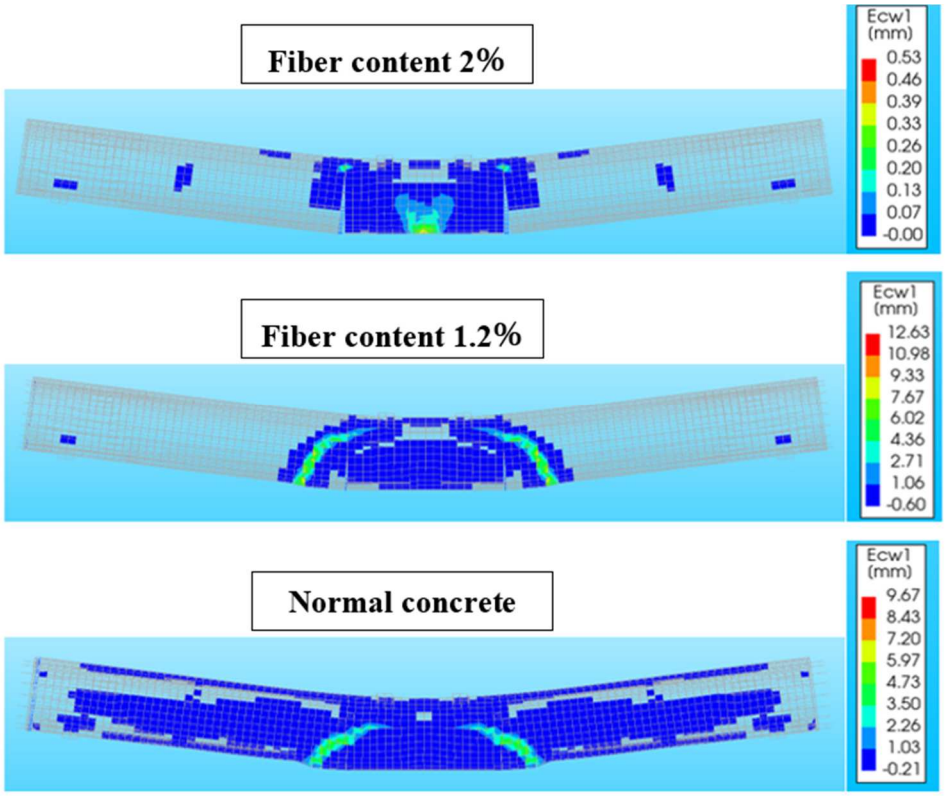

Figure 14: Cracking behavior of all specimens at the peak load

made of normal concrete also presents a bilinear behavior followed by the failure of the specimen. However, the specimen made from normal concrete presents a lower flexural stiffness than the two other specimens, namely specimens with 1.2% and 2% fiber content.

4.2 Cracks propagation

Figure 14 shows the cracking patterns of each specimen at their own peak load.

The specimen with a fiber content of 2% shows only some cracks of 0.39 mm in the middle of the beam. Most of the segments present micro cracks.

However, with a fiber content of 1.2%, the arch mechanism is visible in the UFC concrete. As observed in Figure 14, the crack width of the specimen with a fiber content of 1.2% is around 6 to 7 mm. Also, several micro cracks are observed for this specimen.

The specimen made from normal concrete presents several cracks in the totality of the gross area of concrete. Large diagonal cracks are also observed, with a crack width of 7.2 mm.

5 CONCLUSIONS

The findings of this section could be summarized as follows:

1. The interface parameter obtained with the opening of the experimental results can be used to model the epoxy joint for the large Wind turbine tower. It was observed that specimen S8-JI2 presented a failure pattern, load-deflection, and tensile stress in the PC bars close to the experiment specimen.
2. In the experiment, the specimen does not show a bending failure but instead presents a failure dominated by longitudinal cracks. The analysis explains this by the arch mechanism that occurs when the joint interface opens. Once the interface joint opened, the neutral axis of the cross-section swiftly gradually to the compression side; therefore, the stress transfer in the UFC that allows the equilibrium of the specimen is a compressive stress transfer. This compressive stress transfer generates large lateral stresses leading to those horizontal cracks.
3. As the content of steel fibers reduces

from 2% to 1.2%, the load carrying of the specimen is reduced considerably. Moreover, the failure patterns also changed. The arch mechanism is more visible in the case of specimen with a fiber content of 1.2%.

4. The normal concrete specimen presents large diagonal cracks due to interface opening. Those diagonal cracks are observed in the three segments located in the middle of the beam.

REFERENCES

[1] Xue J, Briseghella B, Huang F, Nuti C, Tabatabai H, Chen B., 2020. Review of ultra-high performance concrete and its application in bridge engineering. *Const. and Build. Mat*, **260**:119844.

[2] Du J., Meng.W., Khayat.K.H., Bao.Y., Guo .P., Lyu .Z., 2021. New development of ultra-high-performance concrete (UHPC). *Compos B Eng.* **224**:109220.

[3] Zhou C, Wang J, Jia W, Fang Z., 2022. Torsional behavior of ultra-high-performance concrete (UHPC) rectangular beams without steel reinforcement: Experimental investigation and theoretical analysis. *Compos Struct*; **299**:116022.

[4] Habel K, Viviani M, Denari´e E, Brühwiler E., 2006. Development of the mechanical properties of an ultra-high performance fiber reinforced concrete (UHPFRC). *Cem Concr Res* **36**(7):1362–70.

[5] Yoo DY, Min KH, Lee JH, Yoon YS., 2014 Shrinkage and cracking of restrained ultra-high-performance fiber-reinforced concrete slabs at early age. *Const. and Build. Mat* **73**:357–65.

[6] Haibo Jiang, Qi Cao, Airong Liu, Tianlong Wang, Yun Qiu., 2016. Flexural behavior of precast concrete segmental beams with hybrid tendons and dry joints. *Const. and Build. Mat*, **110**, 1-7.

[7] Ahmed G.H., Aziz O.Q., 2020. Stresses, deformations and damages of various joints in precast concrete segmental box girder bridges subjected to direct shear loading. *J Eng Struct*, **206**, 11051.

[8] Gopal BA, Hejazi F, Hafezolghorani M, Voo, Y.L., 2020. Shear Strength of Dry and Epoxy Joints for Ultra-High-Performance Fiber-Reinforced Concrete. *ACI Struct J.* **117**(1), pp.279-289, 2020.

[9] Zheng, H., Chen, D., Ou, M., Liang, X., Luo, Y., 2023. Flexural Behavior of Precast UHPC Segmental Beams with Unbonded Tendons and Epoxy Resin Joints. *Buildings,* **13**, 1643.

[10] Rabotovao A. M., Miki, T., 2024. Study on Bending Behavior of Hollow Segmental Circular UFC Beams prestressed with Ungrouted PC Bars", *Proc. Japan Concrete Institute*, **46**, 571-576.